J Neuropathol Exp Neurol
Vol. 69, No. 2
February 2010
pp. 196–206

ORIGINAL ARTICLE

The Connexin43 C-Terminal Region Mediates Neuroprotection During Stroke

Michael G. Kozoriz, MSc, John F. Bechberger, MSc, Geralyn R. Bechberger, BSc, Michael W.H. Suen, BScH, Alonso P. Moreno, PhD, Karen Maass, PhD, Klaus Willecke, PhD, and Christian C. Naus, PhD

Abstract

Connexin43 plays an important role in neuroprotection in experimental stroke models; reducing the expression of this gap junction protein in astrocytes enhances injury upon middle cerebral artery occlusion (MCAO). Because the C-terminal region of connexin43 is important for channel activity, we carried out MCAO stroke experiments in mice expressing a truncated form of connexin43 (Cx43ΔCT mice). Brain sections were analyzed for infarct volume, astrogliosis, and inflammatory cell invasion 4 days after MCAO. Adult cortices and astrocyte cultures were examined for connexin43 (Cx43) expression by immunohistochemistry and Western blot. Cultured astrocytes were also examined for dye coupling, channel conductance, hemichannel activity, and Ca^{2+} wave propagation. The Cx43ΔCT mice exhibit enhanced cerebral injury after stroke. Astrogliosis was reduced and inflammatory cell invasion was increased in the peri-infarct region in these mice compared with controls; Cx43 expression was also altered. Lastly, cultured astrocytes from Cx43ΔCT mice were less coupled and displayed alterations in channel gating, hemichannel activity, and Ca^{2+} wave properties. These results suggest that astrocytic Cx43 contributed to the regulation of cell death after stroke and support the view that the Cx43 C-terminal region is important in protection in cerebral ischemia.

Key Words: Astrocyte, Connexin, Coupling, Gap junction, Gliosis, Ischemia, Microglia, Stroke.

INTRODUCTION

Intercellular gap junction channels provide cytoplasmic continuity between adjacent cells by allowing ions and molecules less than 1.8 kd to pass (1). The role of gap junctions in stroke is controversial. Some reports suggest that gap junctions allow passage of cytotoxic substances, whereas other authors suggest gap junctions pass required metabolites (e.g. antioxidants, adenosine triphosphate [ATP], glucose) to areas of demand while also buffering cytotoxic levels of excitatory amino acids and ions through the astrocytic syncytium (2, 3). Both theories may be correct, and the ratio of healthy to unhealthy cells may determine whether gap junctions are protective or destructive (2). We have previously shown that selectively knocking out the gap junction protein connexin43 (Cx43) in astrocytes results in larger infarct volumes in a middle cerebral artery occlusion (MCAO) permanent focal stroke model (4), suggesting that astrocytic Cx43 limits damage caused by stroke. In addition to forming gap junctions, unopposed connexins may form hemichannels that are known to release substances such as ATP, glutamate, and glutathione (5, 6). Hemichannel activity has also been shown to play a protective role in hypoxic preconditioning by releasing ATP, which is subsequently converted to adenosine that may protect neighboring neurons (7).

A site of interest in elucidating the neuroprotective role of Cx43 is its C-terminal (CT) region, which exhibits several phosphorylation sites that are believed to play a role in gap junction assembly and activity (8, 9). Gating of the Cx43 channel caused by intracellular acid loads is also thought to involve the CT (10). Moreover, the Cx43CT binds to other proteins such as α-tubulin, β-tubulin, CCN3, c-*src*, and zona occludens 1 (8). Given the wide range of interactions, we were interested in determining whether truncation of the gate of Cx43 alters cellular injury during stroke.

In this study, we used mutant mice in which the CT of Cx43 has been truncated at amino acid residue 258 (Cx43ΔCT) (11). Truncation of this region removes casein kinase 1, protein kinase A, protein kinase C, and most of

From the Department of Cellular and Physiological Sciences, Life Sciences Institute, University of British Columbia (MGK, JFB, GRB, MWHS, CCN), Vancouver, British Columbia, Canada; Nora Eccles Cardiovascular MCA Research and Training Institute, University of Utah (APM), Salt Lake City, Utah; Department of Medicine, Langone Medical Center, New York University (KM), New York, New York; and Institut für Genetik, Rheinische Friedrichs-Wilhelm, Universitaet Bonn (KW), Bonn, Germany.

Send correspondence and reprint requests to: Christian C. Naus, PhD, Department of Cellular and Physiological Sciences, Life Sciences Institute, The University of British Columbia, 2350 Health Sciences Mall, Room 1352, Vancouver, British Columbia, Canada V6T 1Z3; E-mail: cnaus@interchange.ubc.ca

This work was funded by the Heart and Stroke Foundation of British Columbia and Yukon, Canada to Christian C. Naus and by grants of the German Research Association through the Research Group on Keratinocytes and through SFB 645, B2, to Klaus Willecke. Michael G. Kozoriz is supported by a CIHR-Vancouver Coastal Health Research Institute-UBC MD/PhD Studentship Award and by the Michael Smith Foundation for Health Research. This work was also supported by NIH R01 HL63969 and by the Nora Eccles Harrison Treadwell Foundation to Alonso P. Moreno. Christian C. Naus is a Canada Research Chair.

Supplemental digital content is available for this article. Direct URL citations appear in the printed text and are provided in the HTML and PDF versions of this article on the journal's Web site (www.jneuropath.com).

Online-only figures are available at http://www.jneuropath.com.

the mitogen-activated protein kinase phosphorylation sites; the *src* homology 2, *src* homology 3, and the PDZ zona occludens 1 binding domains are also removed. Interaction sites for microtubules are preserved in this mutant, as are a $p34^{cdc2}$, mitogen-activated protein kinase, and *src* phosphorylation site (8, 12–17). Cells with the Cx43ΔCT mutation are known to electrically couple, but single-channel recording in cardiomyocytes reveals a lack of the 30 pS substate and prolonged channel opening times (18). Similar truncations of the CT are also known to cause disruption of channel gating (19).

Because of the broad functions attributed to Cx43, in this initial study we sought to determine the importance of the CT region of Cx43 in stroke by examining several processes relevant to stroke. We tested the susceptibility to cellular injury, astrogliosis, and inflammatory cell invasion in Cx43ΔCT mice after MCAO. Furthermore, we explored the expression and functional properties of Cx43ΔCT in adult cortices and cultured astrocytes.

MATERIALS AND METHODS

All experiments were performed in accordance with the guidelines established by the Canadian Council on Animal Care and were approved by The University of British Columbia Animal Care Committee.

Knockout Mice and MCAO

Mice from a 129/Ola/C57BL/6 genetic background in which Cx43 has been replaced by Cx43K258stop ($Cx43^{\Delta CT}$) (11) were used. Breeding and genotyping of $Cx43^{+/+}$, $Cx43^{+/-}$, $Cx43^{\Delta CT/+}$, $Cx43^{\Delta CT/-}$, and $Cx43^{\Delta CT/\Delta CT}$ mice have been previously described (11, 18, 20). $Cx43^{\Delta CT/\Delta CT}$ mice are not viable because of an epidermal barrier defect (11), but it is possible to culture $Cx43^{\Delta CT/\Delta CT}$ astrocytes near birth. Details of the MCAO surgeries are described in our previous studies (4, 21, 22). In brief, 8- to 10-week-old mice were anesthetized with sodium pentobarbital (65 mg/kg intraperitoneally [i.p.]; MTC Pharmaceuticals, Cambridge, Ontario, Canada). Once they were unconscious, hair over the surgery site was cut with an electric razor, and the mice were secured to a 37°C heating pad and placed in a stereotaxic frame. A skin incision was made, and the squamosal bone was exposed by retracting the temporalis muscle. A 3-mm burr hole was made over the MCA with a Dremel drill using a no. 105 engraving cutter drill bit (Robert Bosch Tool Corp, Mount Prospect, IL). The dura mater was pierced with a needle, and the MCA was occluded above and below the rhinal fissure by electrocautery. The skin incision was closed with sutures, and the mice were kept in a cage warmed on a 37°C heating pad until they regained consciousness.

Infarct Volume

At 4 days after MCAO, the mice were anesthetized with sodium pentobarbital (70 mg/kg i.p.) and were transcardially perfused with PBS followed by perfusion with 10% formalin (Sigma-Aldrich, Oakville, Ontario, Canada). Brains were removed and placed in 10% formalin overnight then stored in a 10% formalin-30% sucrose solution. Using a cryostat (HM 505E; Micron, Walldorf, Germany), 20-μm-thick brain slices were collected every 100 μm and mounted sequentially on glass microscope slides. To measure infarct sizes, sections were stained with 0.125% thionin (Fisher Scientific, Ottawa, Ontario, Canada). Quantification of the infarct volume consisted of adding together the measured lesion area in each section as previously described using Scion Image Software (Scion Corporation, Frederick, MD) (21, 22).

Examination of Brain Vasculature

To visualize brain vasculature, 8- to 10-week-old mice were anesthetized with sodium pentobarbital (65 mg/kg i.p.) and were transcardially perfused with PBS then 10% formalin followed by 3 to 5 mL of a staining solution containing 3.5 g gelatin (Fisher Scientific) dissolved in 60 mL water, plus 10 mL of 25% mannitol (Sigma-Aldrich) and 20 mL of india ink (Speedball Art Company, Houston, TX) (23). The mice were stored at 4°C for 24 hours to allow for solidification of the gelatin, after which the brains were extracted and stored in 10% formalin. Dark ink-filled blood vessels were apparent using this protocol, and brains were photographed using a digital camera (Canon Powershot SD750; Canon Inc, Mississauga, Ontario, Canada). To examine the microvasculature in these mice, 50-μm coronal sections were obtained using a vibratome (Campden Instruments, Lafayette, IN). Sections were mounted on glass slides and stained with 1% neutral red (Sigma-Aldrich) for 5 minutes, followed by washes in water, 50% ethanol, 70% ethanol, 100% ethanol (twice), and 100% xylene (twice) (24). Slides were mounted using Cryoseal XYL (Richard-Allan Scientific, Kalamazoo, MI), and images were obtained on a Leica microscope (Leica Microsystems, Richmond Hill, Ontario, Canada).

Astrocyte Cultures

Neonatal (0–1 day) brains were removed from mice and placed in PBS. Neocortices were isolated, freed of meninges, and placed in high-glucose Dulbecco modified Eagle medium (Invitrogen, Burlington, Ontario, Canada) supplemented with 10% fetal bovine serum (HyClone, Logan, UT), 10 U/mL penicillin, and 10 U/mL streptomycin (Invitrogen). Tissue was mechanically disrupted and passed through a 70-μm cell strainer (BD Falcon, Bedford, MA). Cells were resuspended in high-glucose Dulbecco modified Eagle medium supplemented with 10% fetal bovine serum, 10 U/mL penicillin, and 10 U/mL streptomycin, and maintained in a humidified incubator in 95% air/5% carbon dioxide at 37°C. A fresh medium change was performed every 4 days (25). Confluent cells were passed onto glass coverslips or plastic culture dishes, and astrocytes were used between 14 and 21 days in vitro.

Immunohistochemistry

Immunohistochemistry was performed as previously described on brain tissue obtained 4 days after MCAO and after fixation with 4% paraformaldehyde (Sigma-Aldrich) (4, 21, 26). In brief, 10-μm glass-mounted sections were rinsed in PBS and exposed to 0.3% Triton X-100 (Fisher Scientific) in PBS for 2 minutes. After a brief rinse in PBS, cells were blocked in 5% normal goat serum ([NGS] Sigma-Aldrich) for 30 minutes. Sections were then incubated overnight in 1.5% NGS-PBS and primary antibody. Sections were

then washed 3 times for 10 minutes with PBS and subsequently incubated for 1 hour with the secondary antibody. After incubation, slides were rinsed 3 times for 10 minutes with PBS, dipped in water, and mounted with ProLong Gold antifade reagent with 4′,6-diamidino-2-phenylindole ([DAPI] Molecular Probes, Eugene, OR). Control experiments were performed by omitting the primary antibodies and by incubating the primary antibody with the opposite secondary. Primary antibodies were used at the concentrations indicated: anti-Cx43 C-terminal (amino acid residues 363–382) raised in rabbit (1:2000 dilution, catalogue no. C6219; Sigma-Aldrich), anti-Cx43 cytoplasmic loop (amino acids residues 131–142) raised in mouse (1:50, catalogue no. 05-763; Upstate, Lake Placid, NY), anti-glial fibrillary acidic protein (GFAP) raised in mouse (1:1000, catalogue no. G3893; Sigma-Aldrich) and anti-ionized calcium-binding adaptor molecule 1 (IBA-1) produced in rabbit (1:500, catalogue no. 019-19741; Wako Pure Chemical Industries, Richmond, VA). Secondary antibodies consisted of a 1:500 dilution of highly cross-adsorbed goat anti-rabbit or anti-mouse IgG conjugated to Alexa Fluor 488 (catalogue no. A-11029 and no. A-11034) or Alexa Fluor 568 (catalogue no. A-11031 and no. A-11036) used as appropriate (Molecular Probes). All images were obtained on a Zeiss Axioplan2 fluorescence microscope (Carl Zeiss Ltd, Toronto, Canada).

Immunocytochemistry on astrocyte cultures was performed as previously described using the same concentration of Cx43 antibodies and secondary antibodies (27). In brief, astrocytes were rinsed in PBS, fixed in 4% paraformaldehyde, briefly rinsed in PBS, and then exposed to 0.1% Triton-X-100 PBS (Fisher Scientific) for 2 minutes. After a brief rinse, cells were blocked in 5% NGS for 20 minutes. Astrocytes were then incubated for 1 hour in PBS containing 1.5% NGS and primary antibody. Astrocytes were then washed 3 times for 10 minutes with PBS and subsequently incubated for 1 hour with a secondary antibody. After incubation, astrocytes were rinsed 3 times for 10 minutes with PBS, dipped in water, and mounted with ProLong Gold with DAPI.

Western Blot

Adult brain samples and astrocyte cultures were prepared and probed as previously described (18). In brief, tissue was lysed in Laemmli buffer supplemented with Complete Mini (Roche, Indianapolis, IN) and phosphatase inhibitors (Sigma-Aldrich), and the samples were drawn up by a syringe through a 26-gauge needle. Samples were then sonicated and centrifuged at 10,000 × *g* for 10 minutes. Protein concentrations were determined using a BCA protein quantification kit (Pierce, Rockford, IL). Protein samples (30 μg) were heated at 37°C for 30 minutes in Laemmli buffer and loaded onto a 12% polyacrylamide gel for separation. Protein was then transferred to a nitrocellulose membrane. The membrane was blocked in 5% milk in Tris-buffered saline with Tween (TBS-T) for 1 hour followed by incubation in a primary antibody in 5% milk and TBS-T overnight. The blot was washed 3 times in TBS-T for 10 minutes and then incubated in secondary antibody. Next, the blot was washed 3 times in TBS-T for 10 minutes and was placed in TBS for 5 minutes. Protein was detected by exposing the blot to Super-Signal chemiluminescent substrate (Pierce). Note that when the anti-Cx43 N-terminal antibody was used, all incubations were in 1% milk and in the absence of Tween. Primary antibodies were used at the following dilutions: anti-Cx43 C-terminal (1:8000), anti-Cx43 N-terminal clone P1E11 (1:300; amino acid residues 1–19; Fred Hutchinson Cancer Research Center, Seattle, WA), anti-Cx43 cytoplasmic loop (1:200), Cx30 (1:250, catalogue no. 71-2200; Zymed, San Francisco, CA) and anti-glyceraldehyde 3-phosphate dehydrogenase ([GAPDH] 1:10,000, catalogue no. 5G4 MAb 6C5; HyTest, Turku, Finland). The secondary antibodies, goat anti-mouse or anti-rabbit horseradish peroxidase-tagged, were used at a 1:3000 dilution (catalogue no. A6154 and no. A8924; Sigma). To ensure equal loading of protein samples, the blots were stripped and reprobed for GAPDH.

Astrogliosis and Inflammatory Cell Measurements

Ten-micrometer-thick sections from mice subjected to MCAO were probed with a low concentration of anti-GFAP antibody to stain reactive astrocytes (21, 26). Micrographs were obtained along the lateral border of the section under a 16× objective from the edge of necrosis to the edge of astrogliosis, where reactive astrocyte staining was similar to that of the rest of the section (21, 26); each 16× field corresponded to 550 μm × 550 μm area. For each mouse, the extent of astrogliosis was determined by averaging 5 measurements from the necrotic edge to the edge of astrogliosis in 3 separate sections.

To quantify the extent of inflammatory cells in the peri-infarct region of the stroke, 10-μm-thick sections were labeled with anti–IBA-1 to detect microglia and infiltrated blood-derived macrophages. Sections (n = 3 per mouse) were examined under 16× magnification. In each section, cells were counted in 3 randomly chosen fields in the region adjacent to the edge of necrosis, and data from each field were averaged (21).

Gap Junction Coupling

To assess the extent of gap junction coupling, cells were incubated with 50 μL of gap junction–permeable carboxyfluorescein (0.1%) and gap junction–impermeable dextran-rhodamine (0.1%; Molecular Probes) in PBS. Cells were scraped with a scalpel blade and allowed to incubate for 2 minutes after which excess dye was washed off with PBS. A gap junction blocker, carbenoxolone ([CBX] 20 μmol/L; Sigma-Aldrich), was then added to inhibit further coupling. The distance carboxyfluorescein traveled from the source cells was taken as a measure of the extent of coupling.

Electrophysiology

A dual whole-cell voltage clamp technique was applied to cell pairs to measure their junctional conductance (g_j). The patch solution consisted of (in mmol/L) 130 $CsCl_2$, 0.5 $CaCl_2$, 2 Na_2ATP, 3 MgATP, 10 4-(2-hydroxyethyl)-1-piperazine ethanesulfonic acid (HEPES), 10 EGTA, pH 7.2. The recording solution consisted of (in mmol/L) 130 NaCl,

7 $CsCl_2$, 2.0 $CaCl_2$, 0.6 $MgCl_2$, 10 HEPES, pH 7.4. Single-channel currents were measured using freshly plated astrocytes on glass covers slips. Unitary junction currents were observed after 30-second superfusion of 2 mmol/L halothane and digitized during long-voltage steps applied to one of the cells. Amplitudes of unitary opening or closing current events were digitized through a HEKA 9000 amplifier (HEKA, Lambrecht, Germany) filtered at 200 Hz. Probability distribution histograms of the events and Gaussian distribution best fits for each peak were calculated for each experiment (Origin 7.0; OriginLab Corporation, Northampton, MA). Single-channel current traces were digitized at 5 kHz, filtered at 100 Hz, and used to generate all point histograms with a bin resolution of 0.5 to 2.5 pS.

Hemichannel Assay

Hemichannel activity was assessed by propidium iodide uptake (7). Cells were washed with Hanks buffered salt solution (Invitrogen Corp) with Ca^{2+} and then incubated in Hanks buffered salt solution with or without Ca^{2+}containing 1.5 mmol/L propidium iodide for 15 minutes. Cells were then washed 3 times with Hanks buffered salt solution and were fixed and mounted on glass slides for subsequent analysis. Carbenoxolone was also applied 5 minutes before and during the experiment in a portion of cells to test the specificity of hemichannel openings.

Calcium Imaging

Confluent astrocytes were placed in imaging buffer (in mmol/L): 136.5 NaCl, 3.0 KCl, 1.5 NaHCO3, 1.5 MgSO4, 10.0 D-glucose, 2.0 $CaCl_2$, and 10.0 HEPES with 5 μmol/L fura-2 AM (Molecular Probes) for 1 hour at room temperature. After washing, the cells were mounted in a perfusion chamber on a Zeiss Axioskop2 FS Plus microscope (Carl Zeiss Canada Ltd). Measurement of $[Ca^{2+}]_i$ was performed using the dual excitation ratio method (340 and 380 nm; Lambda DG-5, Sutter Instrument Co, Novato, CA) under a 20× objective, and fluorescence emissions greater than 505 nm were captured by a 12-bit digital cooled CCD camera every 5 seconds (Retiga EXi, QImaging, Burnaby, Canada) and analyzed offline using SlideBook (version 4.1 Intelligent Imaging Innovations, Denver, CO). Calcium waves were generated by mechanical stimulation (20, 28). The following 3 parameters were measured: the distance of Ca^{2+} wave propagation (measured as the distance between the stimulated cell and the furthest activated cell); the wave velocity (calculated by dividing the furthest distance by the time interval taken to reach that astrocyte); and the efficacy of the Ca^{2+} spread (calculated as the number of activated cells divided by the total number of cells).

Data Analysis

Results are reported as means ± SE. Statistical comparisons were performed using a one-way analysis of variance with a Student-Newman-Keuls multiple comparisons test, with a 95% confidence limit.

RESULTS

Given the importance of gap junctions in brain cellular injury (29) and the role of the CT region of Cx43 in channel gating, we sought to determine the significance of the Cx43ΔCT mutation during stroke after MCAO. In comparison with wild-type mice, infarct volumes were greater in $Cx43^{+/-}$, $Cx43^{\Delta CT/+}$, and $Cx43^{\Delta CT/-}$ mutant mice ($p < 0.05$) (Fig. 1). Moreover, infarct volumes from $Cx43^{+/+}$ mice were compared with $Cx43^{\Delta CT/+}$ mice, and $Cx43^{+/-}$ mice were compared with $Cx43^{\Delta CT/-}$ mice, and in both instances, the presence of the Cx43ΔCT mutation conferred a larger infarct volume (Fig. 1), and no differences were observed between $Cx43^{\Delta CT/+}$ and $Cx43^{\Delta CT/-}$ mice ($p > 0.05$). The vasculature of each genotype was examined by filling blood vessels with india ink. Although brain vascularization patterns were variable within each genotype at the gross and microvasculature levels, no obvious vessel abnormalities were detectable across the 4 genotypes (Figure, Supplemental Digital Content 1, http://links.lww.com/NEN/A82).

Astrocytes increase their GFAP expression and interweave to form a gliotic scar after a stroke (30), and Cx43 is known to be increased in reactive and proliferating astrocytes after stroke (31). We previously showed that $Cx43^{+/-}$ mice exhibit reduced astrogliosis after MCAO (21, 26). In $Cx43^{+/+}$ mice, the region of gliosis extended 891 ± 69 μm from the necrotic core (n = 6). As in our previous studies, gliotic region was significantly reduced (to 591 ± 77 μm) in $Cx43^{+/-}$ mice (n = 6, $p < 0.05$). Gliosis was further reduced to 558 ± 98 μm and 500 ± 31 μm in $Cx43^{\Delta CT/+}$ and $Cx43^{\Delta CT/-}$ mice,

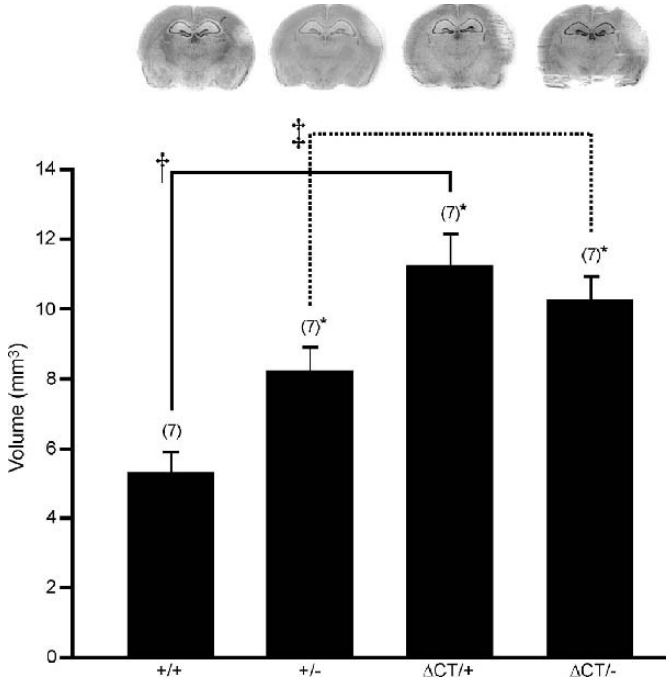

FIGURE 1. The Cx43ΔCT mutation results in increased infarct size after middle cerebral artery occlusion (MCAO). Infarct volumes after MCAO were increased in $Cx43^{+/-}$, $Cx43^{\Delta CT/+}$, and $Cx43^{\Delta CT/-}$ mice compared with $Cx43^{+/+}$ mice (*$p < 0.05$). Infarcts were also larger in $Cx43^{\Delta CT/+}$ mice compared with $Cx43^{+/+}$ mice (†$p < 0.05$); and $Cx43^{\Delta CT/-}$ infarcts were larger when compared with $Cx43^{+/-}$ infarcts (‡$p < 0.05$). Numbers of mice in each group are indicated. Representative coronal sections showing infarcts corresponding to each group are shown above the graph.

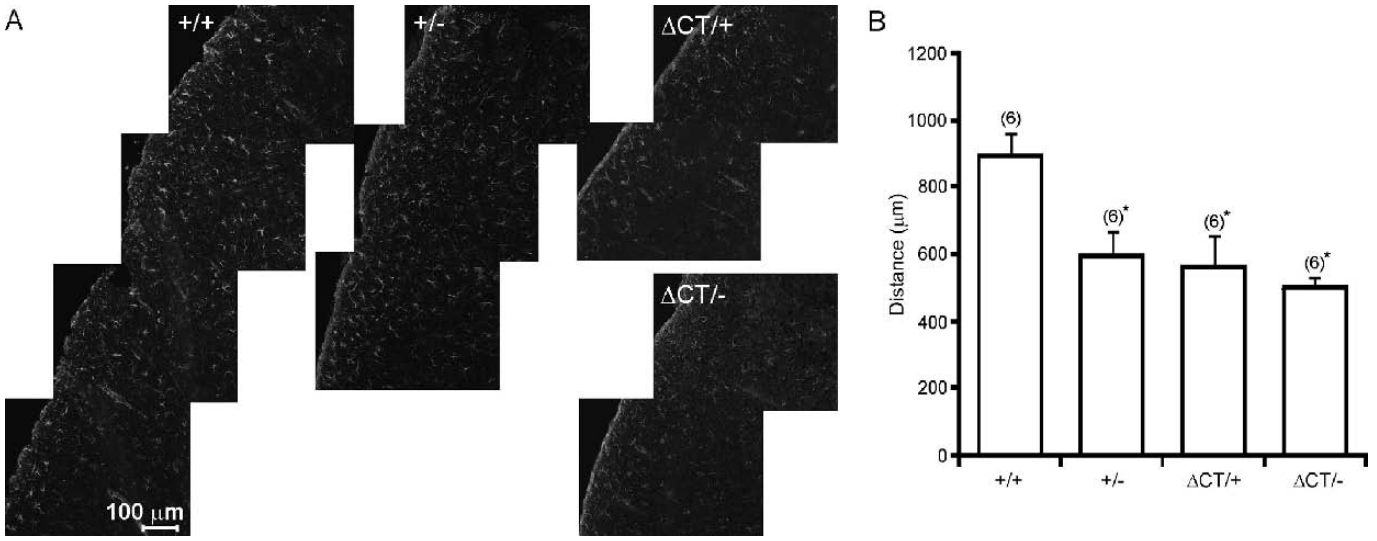

FIGURE 2. Reactive astrogliosis is decreased in Cx43ΔCT mice. **(A)** Staining for glial fibrillary acidic protein revealed a decrease in the extent of astrogliosis in the peri-infarct region of $Cx43^{+/-}$, $Cx43^{\Delta CT/+}$, and $Cx43^{\Delta CT/-}$ mice. **(B)** Graph quantifying the degree of astrogliosis indicated by the distance of the gliosis (extent) from the necrotic core in each of the genotypes tested (*$p < 0.05$ in comparison with $Cx43^{+/+}$). There was no significant difference between $Cx43^{\Delta CT/+}$ and $Cx43^{\Delta CT/-}$ mice, $p > 0.05$. Numbers of animals in each group are indicated.

respectively ($n = 6$, $p < 0.05$; Figs. 2A, B), suggesting that disruption of the CT region of Cx43 interferes with glial scar formation.

Microglial/macrophage responses in infarcts can be beneficial or harmful depending on the inflammatory context (32). Ablation of proliferating microglia is known to increase ischemic injury (33), and microglia are known to effect gap junctional communication (34–36). Furthermore, microglia express Cx43 and Cx36 (37, 38). Cx43ΔCT mice are known to have increased inflammation and neutrophil recruitment in an inflammatory lung model (39), and previous studies have shown that microglial invasion is increased in the penumbral region after MCAO in $Cx43^{+/-}$ mice (21). Here, we found that the Cx43ΔCT mutation leads to changes in microglia/macrophage (IBA-1–labeled) cells in the peri-infarct region after stroke. In wild-type brains, there were 27 ± 3.9 inflammatory cells per 16× field of view ($n = 6$). Inflammatory cell invasion was greater in $Cx43^{+/-}$ (43 ± 5.3 cells, $n = 6$; $p < 0.05$), $Cx43^{\Delta CT/+}$ (50 ± 7.0 cells, $n = 6$; $p < 0.05$), and $Cx43^{\Delta CT/-}$ (52 ± 3.1 cells, $n = 6$; $p < 0.05$) brain sections

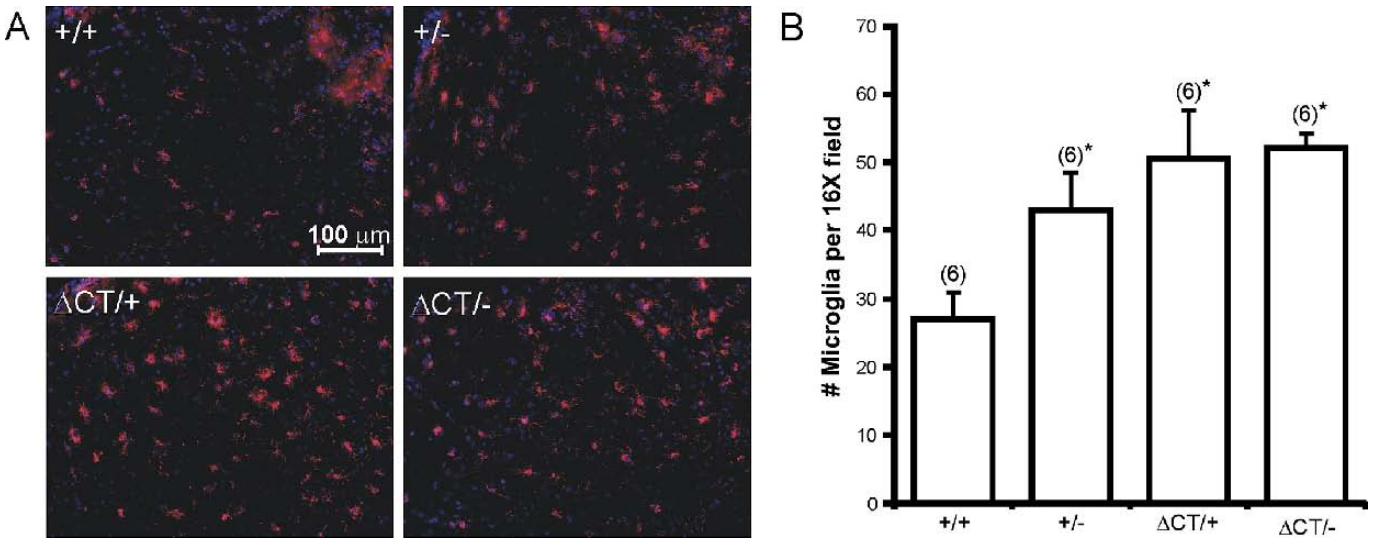

FIGURE 3. The inflammatory reaction is increased in Cx43ΔCT mice. **(A)** Ionized calcium-binding adaptor molecule 1 staining (red) revealed an increase in microglia/macrophages in the penumbral region of $Cx43^{+/-}$, $Cx43^{\Delta CT/+}$, and $Cx43^{\Delta CT/-}$ compared with control mice. Nuclei are labeled with DAPI (blue). **(B)** Graph quantifying the number of microglia/macrophages in each of the genotypes tested (*$p < 0.05$ in comparison with $Cx43^{+/+}$. There was no significant difference observed between $Cx43^{\Delta CT/+}$ and $Cx43^{\Delta CT/-}$ mice, $p > 0.05$). Numbers of mice in each group are indicated.

(Figs. 3A, B). Microglia/macrophages in the peri-infarct region had morphology consistent with those of activated microglia (40, 41).

Immunostaining of astrocyte cultures (Figs. 4A, B) and brain sections (Figs. 4C, D) using antibodies against the C-terminal and cytoplasmic loop of Cx43 revealed typical membrane localization in $Cx43^{+/+}$ cells and less expression in $Cx43^{+/-}$ cells, as previously reported (20). Membrane localization was also observed in $Cx43^{\Delta CT/+}$ astrocytes with both antibodies (Fig. 4), but more distinct immunolabeled gap junction plaques were observed, and cytoplasmic staining remained sparse. Plaques were also observed in $Cx43^{\Delta CT/-}$ astrocytes using the cytoplasmic loop antibody, but expression seemed reduced overall (Figs. 4B, D). No staining was observed using the C-terminal antibody in these sections because the corresponding epitope is lacking (Figs. 4A, C). Therefore, the use of the anti–C-terminal antibody in $Cx43^{\Delta CT/\Delta CT}$ cultures resulted in no signal, whereas the cytoplasmic loop antibody revealed overall reduced Cx43 expression, but plaque formation was still maintained (Fig. 4B).

To characterize Cx43 expression further, Western blots were preformed on samples from astrocyte cultures and cortical brain tissue (Fig. 5). The concentrations of Cx43 protein correlated with the intensity of staining observed in Figure 4. Bands representing Cx43 were observed in $Cx43^{+/+}$, $Cx43^{+/-}$, and $Cx43^{\Delta CT/+}$ samples when they were probed with the anti–C-terminus Cx43 antibody. Furthermore, the use of an antibody against the N-terminal of Cx43 resulted in additional bands at approximately 30 kd in the $Cx43^{\Delta CT/+}$, $Cx43^{\Delta CT/-}$, and $Cx43^{\Delta CT/\Delta CT}$ cells, representing the truncated form of Cx43. Cx30 staining was also performed. Staining was observed in adult cortical brain samples, whereas Cx30 was absent in cultured astrocytes, as previously reported. When the density of the Cx30 band was normalized to GAPDH (n = 4) and subsequently normalized to the Cx30 band obtained from $Cx43^{+/+}$ samples, it was found that Cx30 levels were unchanged in $Cx43^{+/-}$ mice (1.004 ± 0.09; $p > 0.05$). Nonsignificant decreases in Cx30 were observed in $Cx43^{\Delta CT/+}$ (0.71 ± 0.15; $p > 0.05$) and $Cx43^{\Delta CT/-}$ (0.76 ± 0.13; $p > 0.05$) tissue.

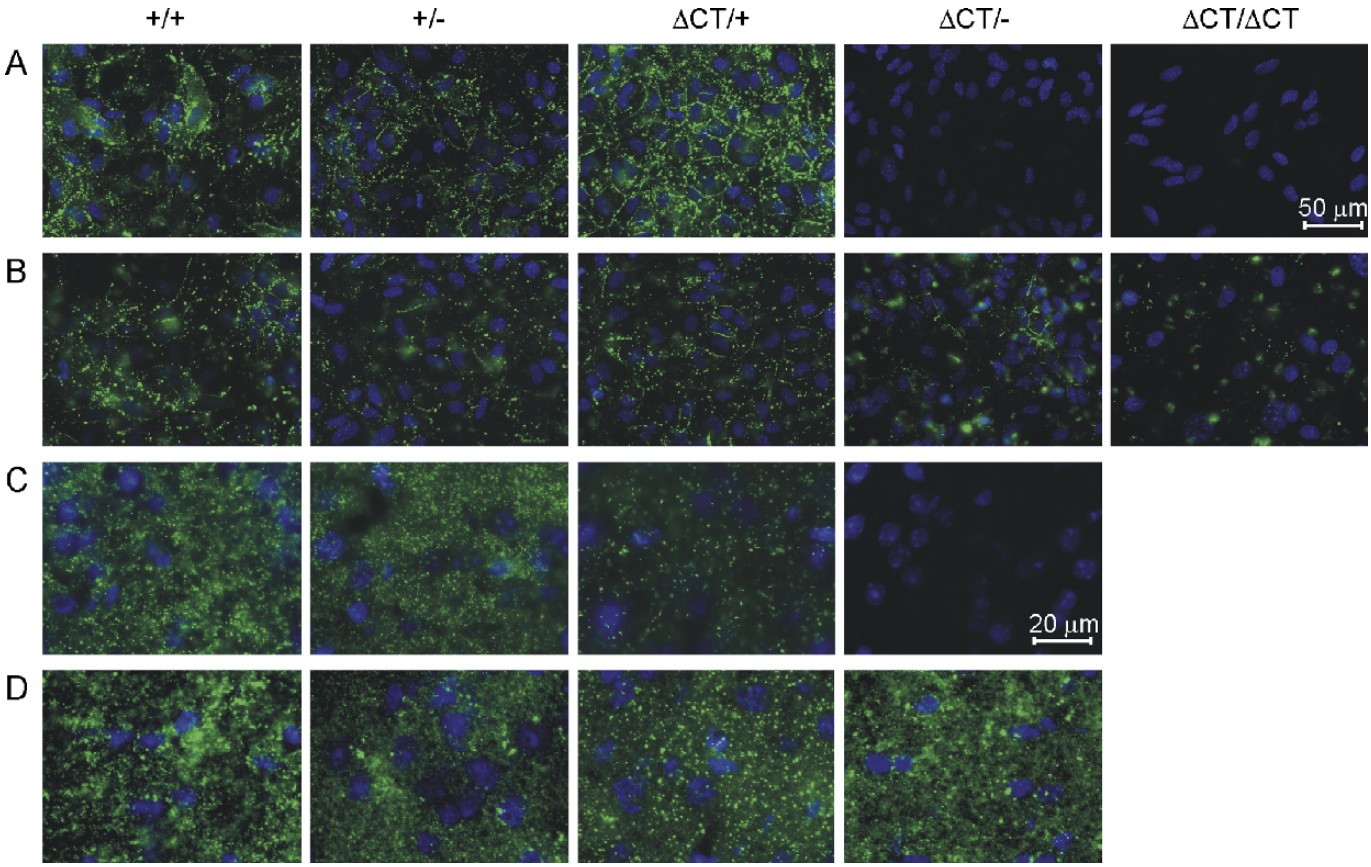

FIGURE 4. Immunohistochemistry for Cx43 in Cx43ΔCT mutants. **(A)** Cultured astrocytes from mice with the indicated genotypes were stained for Cx43 using an antibody raised against the C-terminal of Cx43 (green). Nuclei are labeled with DAPI (blue). Staining was absent in $Cx43^{\Delta CT/-}$ and $Cx43^{\Delta CT/\Delta CT}$ astrocytes because of lack of the C-terminal. **(B)** Cultured astrocytes were also stained with an antibody against the cytoplasmic loop of Cx43. Cx43 plaques appeared to form in all genotypes, but expression was reduced in $Cx43^{+/-}$, $Cx43^{\Delta CT/+}$, $Cx43^{\Delta CT/-}$, and $Cx43^{\Delta CT/\Delta CT}$ genotypes. **(C, D)** Brain sections from the cortical region in the distribution of the middle cerebral artery from the indicated genotypes were stained for Cx43 (green) using an antibody raised against the C-terminal of Cx43 **(C)** and the intracellular loop **(D)**. The staining patterns appear similar to those observed in cultured cells. Because $Cx43^{\Delta CT/\Delta CT}$ mice are not viable, only cultured astrocytes could be evaluated.

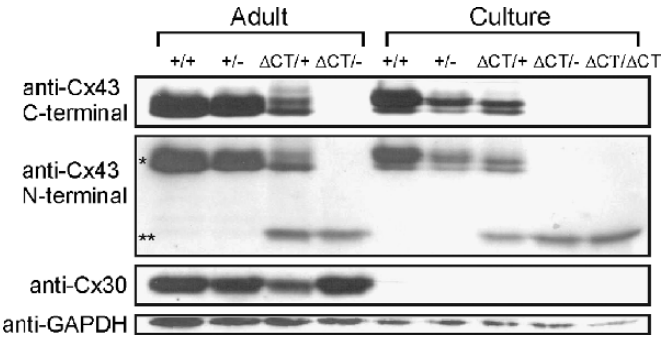

FIGURE 5. Western blot of adult cortex and astrocyte culture tissue. Samples obtained from the cortex of adult mice or cultured astrocytes were stained with the anti-Cx43 C-terminal, anti-Cx43 N-terminal, anti-Cx30, or anti-glyceraldehyde 3-phosphate dehydrogenase (GAPDH) antibodies. Staining with the C-terminal antibody was observed in $Cx43^{+/+}$, $Cx43^{+/-}$, and $Cx43^{\Delta CT/+}$ samples and absent in $Cx43^{\Delta CT/-}$ samples. Using the N-terminal Cx43 antibody, staining of full-length (*) and truncated (**) Cx43 could be observed. In adults, Cx30 expression was similar across the genotypes tested and absent in cultured tissue. GAPDH served as a loading control.

Because gap junctional intercellular communication has been proposed to play a role in stroke (2, 3), confluent cultures of astrocytes were subjected to scrape load assays. In comparison with $Cx43^{+/+}$ cultures, where dye passage extended 160 ± 8 μm from the scrape edge, $Cx43^{+/-}$ and $Cx43^{\Delta CT/+}$ cells exhibited reduced levels of coupling (100 ± 4 μm and 138 ± 10 μm, respectively). Coupling was further reduced in $Cx43^{\Delta CT/-}$ and $Cx43^{\Delta CT/\Delta CT}$ astrocytes (74 ± 13 μm and 72 ± 18 μm, respectively) (Fig. 6A).

Double whole-cell voltage clamp was used to study the electrophysiological properties of Cx43 and Cx43ΔCT. Representative current traces from astrocytes expressing full-length Cx43 are shown in Figures 6B1 and B2. The difference in current calculated from the mean of the peak currents indicates that the total opening of the channel was 110 pS, with a residual state of 20 pS. Astrocytes expressing Cx43ΔCT formed gap junction channels with different electrophysiological properties. As shown in the trace in Figures 6B3 and B4, both recorded channel openings show a conductance of about 110 pS with no residual conductance. Moreover, the open time of these channels is much longer, indicating a reduced sensitivity to transjunctional voltage. These are properties previously reported for C-terminal truncated Cx43 channels in cardiomyocytes and transfected mammalian tumor cells (18, 19).

To determine the extent of hemichannel activity, astrocytes were exposed to the hemichannel-permeable dye propidium iodine under normal and Ca^{2+}-free conditions. Dye uptake was minimal in the presence of Ca^{2+}, as extracellular Ca^{2+} blocks hemichannels (Fig. 6C). To determine if uptake was specific for hemichannels and not a result of cell death, the gap junction blocker CBX was applied. Dye uptake was largely reduced in the presence of this blocker (Fig. 6C), suggesting that the observed responses are mediated by hemichannels. For analysis, the average number of dead cells (i.e. labeled cells under Ca^{2+}-free conditions with CBX) was subtracted from the average number of labeled cells under Ca^{2+}-free conditions in the absence of CBX. Hemichannel activity was greater in $Cx43^{+/\Delta CT}$ astrocytes and less in $Cx43^{+/-}$ and $Cx43^{\Delta CT/-}$ astrocytes in comparison with wild-type astrocytes. No further change in activity was observed in $Cx43^{\Delta CT/\Delta CT}$ astrocytes relative to $Cx43^{\Delta CT/-}$ astrocytes.

Ca^{2+} signaling is important in astrocyte signaling and blood vessel regulation (42). Ca^{2+} waves were generated in culture by mechanical stimulation. The distance of wave travel was reduced in $Cx43^{\Delta CT/-}$ and $Cx43^{\Delta CT/\Delta CT}$ cultures (Fig. 6D1). The fraction of cells activated by mechanical stimulation was reduced in $Cx43^{+/-}$, $Cx43^{\Delta CT/-}$, and $Cx43^{\Delta CT/\Delta CT}$ cultures (Fig. 6D2), and wave velocity was unchanged in all genotypes tested (Fig. 6D3) (43). Representative figures of Ca^{2+} waves in $Cx43^{+/-}$ and $Cx43^{\Delta CT/-}$ cultures are shown in Figures 6E1 and E2.

DISCUSSION

Astrocytes are known to protect neurons during brain ischemia (2). During MCAO, a necrotic core develops that is surrounded by a penumbral region. It is thought that astrocytes

FIGURE 6. Gap junction coupling, electrophysiology, hemichannel activity, and Ca^{2+} waves in culture. **(A1)** Gap junctional communication was measured by the distance of dye passage through scraped confluent cultures. **(A2)** Graph quantifying the distance of dye passage: gap junction coupling was reduced in each of the genotypes tested compared with the wild type (*$p < 0.05$). The numbers of cultures examined are indicated. **(B1)** Junctional currents during an 80-mV pulse for 10 seconds from astrocytes expressing full-length Cx43. **(B2)** Digitized points obtained from the region indicated by the bar in B1 were grouped in 0.025 bins and plotted in the histogram. The main peaks were fitted to Gaussian equations, and the differences between the means indicated a channel total conductance of 110 pS and a residual of 20 pS. **(B3)** Junctional currents in Cx43ΔCT tissue as recorded in B1. **(B4)** Digitized points obtained from the region indicated by the bar in B3 were grouped in 0.05 bins and plotted in the histogram. The main peaks were fitted to Gaussian equations, and the differences between the means indicated channel total conductances of 108 and 113 pS; no residual currents were recorded. **(C)** In comparison with $Cx43^{+/+}$ astrocytes, hemichannel activity is increased in $Cx43^{\Delta CT/+}$ cells (*$p < 0.05$) under Ca^{2+}-free conditions ($-Ca^{2+}$). Under $-Ca^{2+}$ conditions, $Cx43^{+/-}$ and $Cx43^{\Delta CT/-}$ had reduced hemichannel activity (*$p < 0.05$), whereas hemichannel activity was not altered in $Cx43^{\Delta CT/\Delta CT}$ astrocytes ($p > 0.05$). Specificity of dye uptake through hemichannels was tested using the gap junction blocker carbenoxolone (CBX). **(D)** Data under Ca^{2+} conditions ($+Ca^{2+}$) are also plotted. The efficacy of Ca^{2+} wave generation caused by mechanical stimulation was greater in $Cx43^{+/+}$ than in $Cx43^{\Delta CT/-}$ and $Cx43^{\Delta CT/\Delta CT}$ cultures **(D1)**; the distance of Ca^{2+} wave travel was less in $Cx43^{+/-}$, $Cx43^{\Delta CT/-}$, and $Cx43^{\Delta CT/\Delta CT}$ cultures **(D2)**; the velocity of Ca^{2+} wave propagation remained unchanged in each of the genotypes **(D3)**. **(E)** A representative figure of a Ca^{2+} wave experiment in $Cx43^{+/-}$ astrocyte cultures 20 seconds after stimulation at the site indicated (*) **(E1)**. The dashed line indicates the region of astrocytes activated at this time point. **(E2)** Figure is similar to **(E1)** and shows the Ca^{2+} wave in $Cx43^{\Delta CT/-}$ astrocytes.

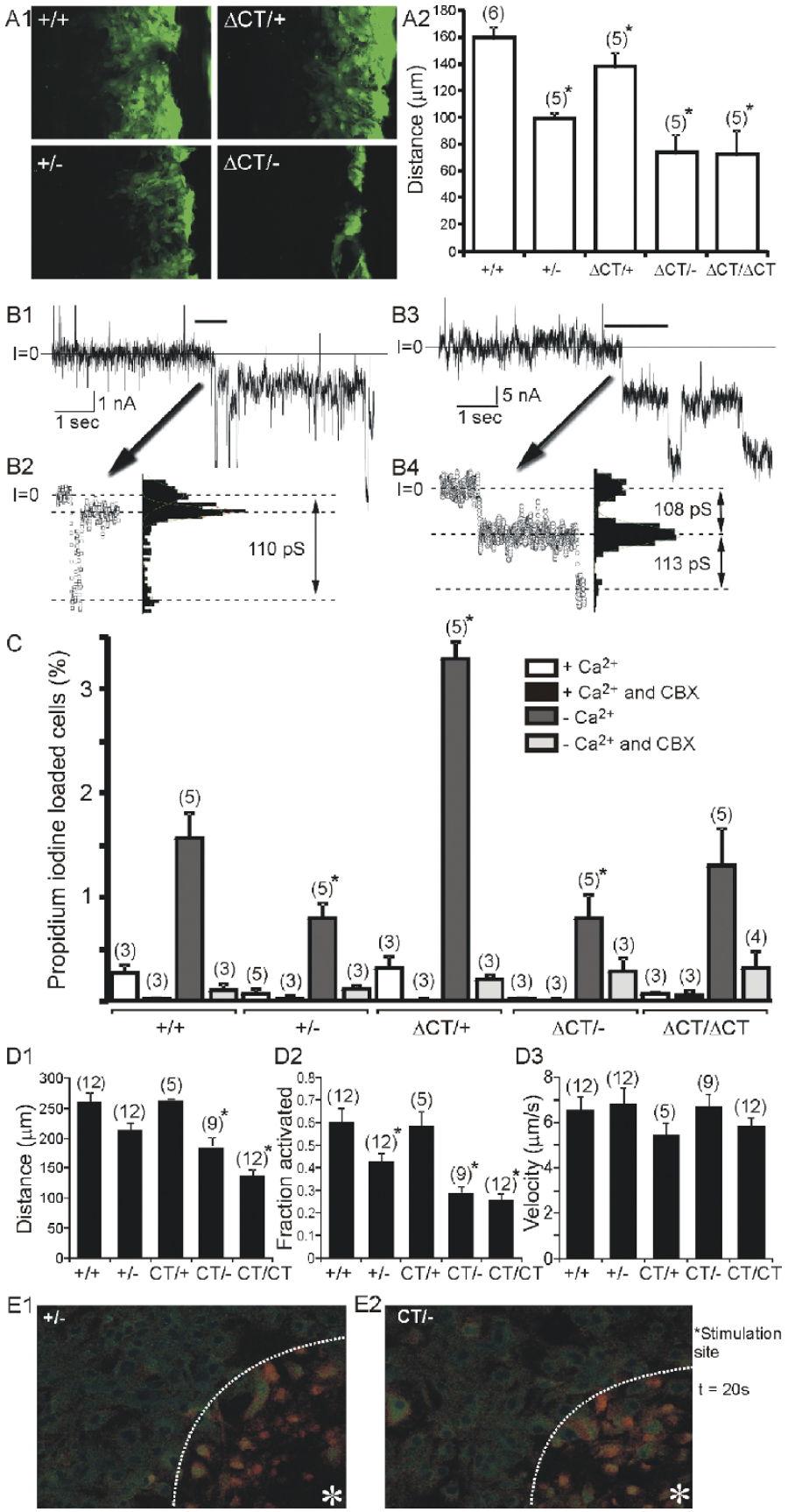

limit the expansion of cell death in the penumbra by buffering cytotoxic substances such as free radicals, glutamate, and K^+, and by providing nutrients such as antioxidants, glucose, and ATP to reduce cellular damage (2, 3). It has been suggested that astrocyte Cx43 plays a role in reducing lesion expansion during stroke (21, 26). The C-terminal of Cx43 is a site of many interacting molecules and is known to be important in channel gating (8, 9, 18, 19). We report that Cx43ΔCT mice display increased stroke damage, suggesting that disruption of the terminal portion of Cx43 significantly alters the ability of astrocytes to protect the brain, and that full-length Cx43 is important for attenuating brain damage.

During stroke, one of the initial events in neurons is a decrease in ATP levels that leads to disruption of ion gradients, including rises in extracellular K^+, intracellular Na^+, intracellular Ca^{2+}, and a decrease in pH. Because astrocytes maintain ATP levels longer, they are less susceptible to ionic disruption (2, 44), but this balance is short-lived when ischemia persists. A reduction in pH is known to close gap junctions, and this gating involves the C-terminal region (10, 45–47). During stroke in wild-type mice, astrocytes would have a decrease in pH that would lead to reduced coupling. This could be beneficial as the passage of cytotoxic molecules to neighboring cells would be reduced (48), but channel gating is impaired in the Cx43ΔCT mice. Interestingly, in this study, the infarct volume in $Cx43^{\Delta CT/+}$ mice was equivalent to that in the $Cx43^{\Delta CT/-}$ mice, suggesting that the Cx43ΔCT mutation could have a dominant negative role in ischemic damage. Therefore, passage of cytotoxic molecules could have led to the enhanced infarct volume observed in these mutants. This scenario does not necessarily negate our previous findings, where reduced expression of Cx43 (hence, less passage of cytotoxic molecules) was found to be destructive during MCAO (4, 21, 22). It is possible that in the early stages of ischemia, gap junction coupling is important for aiding cell survival by allowing the passage of protective molecules such as glucose and antioxidants. It is likely that the ratio of healthy to nonhealthy cells determines whether gap junctions are protective (2), and in the initial stages of stroke, there are more healthy astrocytes in comparison with later stages.

It is unlikely that changes in blood vessel structure contributed to differences in infarct sizes in this study because there were no obvious vessel abnormalities or differences observed when the vessels were filled with india ink. Furthermore, the brain tissue in each of the genotypes under study appeared to be well perfused by microvessels. In addition, another study has shown that after MCAO, there were no differences in cerebral blood flow between $Cx30^{-/-}Cx43^{fl/fl}$: hGFAP-Cre–knockout and wild-type mice (7). Infarct sizes were also unlikely to have been affected by migration of new neural tissue elements at the early time points studied because under conditions that promote generation of new cortical tissue after stroke, NeuN- and BrdU-labeled cells were not detected in infarcts at 3 days and were not significantly appreciable until approximately 11 days after stroke (49).

Our results indicate that in the mutants under study, microglia are increased in the peri-infarct region of the stroke and that astrogliosis is reduced. Cx43 expression is high in infarct regions (50), and it is known to increase in reactive and proliferating astrocytes after stroke (31). The exact role of Cx43 in reactive gliosis is not well described, but it could be involved in coordination of scar formation or through interaction with purinergic receptors involved in cell proliferation and migration (31, 51, 52). Cx43-null mice are known to have reduced expression of P2Y1 receptors (52), and this interaction is believed to involve the C-terminal domain of Cx43 (51). Given the importance of C-terminal involvement, it is not surprising that reduced astrogliosis was found in both Cx43 knockouts (21, 26) and in the Cx43ΔCT mutants used in this study. Activated microglia are known to decrease astrocytic gap junction intercellular communication and increase hemichannel activity (34–36). Because microglial responses were increased in Cx43ΔCT mutants, it is possible that altered communication in the Cx43ΔCT mutants caused a failure to control microglial recruitment that might lead to aggravation of brain tissue injury. It was recently shown that Cx43ΔCT mice have increased inflammation and neutrophil recruitment in a lung injury model (39); activated microglia are known to decrease GFAP expression (53), which correlates with our present findings. Furthermore, microglia themselves have been shown to express Cx43 and to couple (37). Therefore, any disruption of Cx43 (i.e. either reduction of Cx43 or alteration in the C-terminal region) could alter microglia-microglia or microglia-astrocyte signaling processes, thereby resulting in an altered astroglial response. The exact mechanisms involving a Cx43 C-terminal domain interaction require further study.

Full-length Cx43 was found to be reduced in $Cx43^{\Delta CT/+}$ and absent in $Cx43^{\Delta CT/-}$ and $Cx43^{\Delta CT/\Delta CT}$ brain tissue. Cx43ΔCT protein was abundantly expressed in $Cx43^{\Delta CT/+}$, $Cx43^{\Delta CT/-}$, and $Cx43^{\Delta CT/\Delta CT}$ tissue, but despite robust expression of Cx43ΔCT (as detected by Western blot), gap junction plaque formation was reduced. A change in localization and reduction in plaque formation in the heart has also been described in $Cx43^{\Delta CT/-}$ mice (18). The larger plaques are likely caused by a longer Cx43 half-life (11), potentially because of altered degradation, as the C-terminal has been shown to interact with the ubiquitin degradation system (54).

Our data indicate that coupling is reduced in Cx43ΔCT-expressing astrocytes. Although electrophysiological recordings indicate that Cx43ΔCT has a prolonged opening time, the reduced coupling likely reflects a decrease in Cx43 at the plasma membrane. It is important to note that although Cx43ΔCT expression is reduced in the heart in these mutants, whole-cell conduction between cardiomyocytes is not significantly altered in Cx43ΔCT mutants, indicating that there is a large safety factor for proper cell-cell communication under normal conditions (18). Furthermore, heart rates do not differ between $Cx43^{+/-}$ and $Cx43^{\Delta CT/-}$ mice (11).

Astrocyte Ca^{2+} signaling is known to regulate arteriole diameter (42). This may be important in vivo for perfusion of the penumbral region of a stroke. Our data indicate that in $Cx43^{\Delta CT/-}$astrocytes, Ca^{2+} wave distance and efficacy were reduced. Conversely, the Ca^{2+} wave properties studied were unchanged in $Cx43^{\Delta CT/+}$ astrocytes. Ca^{2+} wave propagation depends on both hemichannel activity and gap junction communication (43). Hence, the reduction in coupling observed

may be compensated for by an increase in hemichannel activity.

Hemichannel activity after preconditioning has been proposed to be protective in MCAO, but in the absence of a preconditioning stimulus (as in the present study), hemichannel activity is low (7). In Ca^{2+}-free conditions, only a small proportion of astrocytes displayed hemichannel activity, whereas $Cx43^{\Delta CT/+}$ astrocytes displayed a slight increase in activity. Notably, at physiological Ca^{2+} concentrations, hemichannel activity was negligible (55). Extrapolating to our stroke data, it is unlikely that increased hemichannel activity plays a role in Cx43ΔCT stroke size because increased activity would be expected to decrease infarct volume rather than increase it as we found.

In summary, we found that truncation of the C-terminal of Cx43 increases brain damage caused by experimental MCAO. The consequences of this mutation were broad and included alteration of gliosis, microglial/macrophage response, coupling, channel gating, hemichannel activity, Ca^{2+} waves, and Cx43 expression and localization. Based on comparisons between $Cx43^{+/+}$ and $Cx43^{-/-}$ astrocytes (56), it is also likely that changes in gene expression occur as well (56). Determining which of these processes is most important in stroke pathology is complex, and there are differences between the in vitro and in vivo systems under study (i.e. Cx30 expression in the latter). Unlike our studies of $Cx43^{+/-}$ mice (22), however, truncation of the C-terminal involves disruption of the gating region of Cx43 without the approximately 50% reduction in Cx43 expression observed in the $Cx43^{+/-}$ studies. This ΔCT mutant allows us to study whether the pore of Cx43 is sufficient for protection or whether the C-terminal region is necessary for protection. Gap junction activity and/or interactions at the CT may affect the ultimate outcome of a stroke.

ACKNOWLEDGMENT

The authors thank Noo-Rie Ha for providing technical support for this project.

REFERENCES

1. Neijssen J, Herberts C, Drijfhout JW, et al. Cross-presentation by intercellular peptide transfer through gap junctions. Nature 2005;434:83–88
2. Rossi DJ, Brady JD, Mohr C. Astrocyte metabolism and signaling during brain ischemia. Nat Neurosci 2007;10:1377–86
3. Contreras JE, Sanchez HA, Veliz LP, et al. Role of connexin-based gap junction channels and hemichannels in ischemia-induced cell death in nervous tissue. Brain Res Brain Res Rev 2004;47:290–303
4. Nakase T, Fushiki S, Sohl G, et al. Neuroprotective role of astrocytic gap junctions in ischemic stroke. Cell Commun Adhes 2003;10:413–17
5. Stridh MH, Tranberg M, Weber SG, et al. Stimulated efflux of amino acids and glutathione from cultured hippocampal slices by omission of extracellular calcium: Likely involvement of connexin hemichannels. J Biol Chem 2008;283:10347–56
6. Kang J, Kang N, Lovatt D, et al. Connexin 43 hemichannels are permeable to ATP. J Neurosci 2008;28:4702–11
7. Lin JH, Lou N, Kang N, et al. A central role of connexin 43 in hypoxic preconditioning. J Neurosci 2008;28:681–95
8. Herve JC, Bourmeyster N, Sarrouilhe D, et al. Gap junctional complexes: From partners to functions. Prog Biophys Mol Biol 2007;94:29–65
9. Lampe PD, Lau AF. The effects of connexin phosphorylation on gap junctional communication. Int J Biochem Cell Biol 2004;36:1171–86
10. Duffy HS, Sorgen PL, Girvin ME, et al. pH-dependent intramolecular binding and structure involving Cx43 cytoplasmic domains. J Biol Chem 2002;277:36706–14
11. Maass K, Ghanem A, Kim JS, et al. Defective epidermal barrier in neonatal mice lacking the C-terminal region of connexin43. Mol Biol Cell 2004;15:4597–608
12. Zucker SN, Nicholson BJ. Mutagenic approaches to modifying gap junction phenotype. Curr Drug Targets 2002;3:441–53
13. Lampe PD, TenBroek EM, Burt JM, et al. Phosphorylation of connexin43 on serine368 by protein kinase C regulates gap junctional communication. J Cell Biol 2000;149:1503–12
14. Lampe PD, Lau AF. Regulation of gap junctions by phosphorylation of connexins. Arch Biochem Biophys 2000;384:205–15
15. Giepmans BN, Moolenaar WH. The gap junction protein connexin43 interacts with the second PDZ domain of the zona occludens-1 protein. Curr Biol 1998;8:931–34
16. Giepmans BN, Hengeveld T, Postma FR, et al. Interaction of c-Src with gap junction protein connexin-43. Role in the regulation of cell-cell communication. J Biol Chem 2001;276:8544–49
17. Kieken F, Mutsaers N, Dolmatova E, et al. Structural and molecular mechanisms of gap junction remodeling in epicardial border zone myocytes following myocardial infarction. Circ Res 2009;104:1103–12
18. Maass K, Shibayama J, Chase SE, et al. C-terminal truncation of connexin43 changes number, size, and localization of cardiac gap junction plaques. Circ Res 2007;101:1283–91
19. Moreno AP, Chanson M, Elenes S, et al. Role of the carboxyl terminal of connexin43 in transjunctional fast voltage gating. Circ Res 2002;90:450–57
20. Naus CC, Bechberger JF, Zhang Y, et al. Altered gap junctional communication, intercellular signaling, and growth in cultured astrocytes deficient in connexin43. J Neurosci Res 1997;49:528–40
21. Nakase T, Sohl G, Theis M, et al. Increased apoptosis and inflammation after focal brain ischemia in mice lacking connexin43 in astrocytes. Am J Pathol 2004;164:2067–75
22. Siushansian R, Bechberger JF, Cechetto DF, et al. Connexin43 null mutation increases infarct size after stroke. J Comp Neurol 2001;440:387–94
23. Berry K, Wisniewski HM, Svarzbein L, Baez S. On the relationship of brain vasculature to production of neurological deficit and morphological changes following acute unilateral common carotid artery ligation in gerbils. J Neurol Sci 1975;25:75–92
24. Hekmatpanah J. Cerebral microvessel perfusion and pathologic alteration of the brain during drowsiness and coma caused by brain tumor: A laboratory study on rats. Surg Neurol 2007;67:564–67
25. Ozog MA, Siushansian R, Naus CC. Blocked gap junctional coupling increases glutamate-induced neurotoxicity in neuron-astrocyte co-cultures. J Neuropathol Exp Neurol 2002;61:132–41
26. Nakase T, Fushiki S, Naus CC. Astrocytic gap junctions composed of connexin43 reduce apoptotic neuronal damage in cerebral ischemia. Stroke 2003;34:1987–93
27. Bates DC, Sin WC, Aftab Q, et al. Connexin43 enhances glioma invasion by a mechanism involving the carboxy terminus. Glia 2007;55:1554–64
28. Venance L, Piomelli D, Glowinski J, et al. Inhibition by anandamide of gap junctions and intercellular calcium signalling in striatal astrocytes. Nature 1995;376:590–94
29. Talhouk RS, Zeinieh MP, Mikati MA, et al. Gap junctional intercellular communication in hypoxia-ischemia-induced neuronal injury. Prog Neurobiol 2008;84:57–76
30. Pekny M, Nilsson M. Astrocyte activation and reactive gliosis. Glia 2005;50:427–34
31. Haupt C, Witte OW, Frahm C. Up-regulation of Connexin43 in the glial scar following photothrombotic ischemic injury. Mol Cell Neurosci 2007;35:89–99
32. Ekdahl CT, Kokaia Z, Lindvall O. Brain inflammation and adult neurogenesis: The dual role of microglia. Neuroscience 2009;158:1021–29
33. Lalancette-Hebert M, Gowing G, Simard A, et al. Selective ablation of proliferating microglial cells exacerbates ischemic injury in the brain. J Neurosci 2007;27:2596–605
34. Retamal MA, Froger N, Palacios-Prado N, et al. Cx43 hemichannels and gap junction channels in astrocytes are regulated oppositely by proinflammatory cytokines released from activated microglia. J Neurosci 2007;27:13781–92

35. Meme W, Calvo CF, Froger N, et al. Proinflammatory cytokines released from microglia inhibit gap junctions in astrocytes: Potentiation by beta-amyloid. FASEB J 2006;20:494–96
36. Kielian T, Esen N. Effects of neuroinflammation on glia-glia gap junctional intercellular communication: A perspective. Neurochem Int 2004; 45:429–36
37. Eugenin EA, Eckardt D, Theis M, et al. Microglia at brain stab wounds express connexin43 and in vitro form functional gap junctions after treatment with interferon-gamma and tumor necrosis factor-alpha. Proc Natl Acad Sci U S A 2001;98:4190–95
38. Dobrenis K, Chang HY, Pina-Benabou MH, et al. Human and mouse microglia express connexin36, and functional gap junctions are formed between rodent microglia and neurons. J Neurosci Res 2005;82:306–15
39. Sarieddine MZ, Scheckenbach KL, Foglia B, et al. Connexin43 modulates neutrophil recruitment to the lung. J Cell Mol Med 2009 [Epub ahead of print]
40. Walz W. *Cerebral Ischemia: Molecular and Cellular Pathophysiology*. Totowa, NJ: Humana Press, 1999
41. Cuadros MA, Navascues J. The origin and differentiation of microglial cells during development. Prog Neurobiol 1998;56:173–89
42. Mulligan SJ, MacVicar BA. Calcium transients in astrocyte endfeet cause cerebrovascular constrictions. Nature 2004;431:195–99
43. Scemes E, Dermietzel R, Spray DC. Calcium waves between astrocytes from Cx43 knockout mice. Glia 1998;24:65–73
44. Silver IA, Deas J, Erecinska M. Ion homeostasis in brain cells: Differences in intracellular ion responses to energy limitation between cultured neurons and glial cells. Neuroscience 1997;78:589–601
45. Liu S, Taffet S, Stoner L, et al. A structural basis for the unequal sensitivity of the major cardiac and liver gap junctions to intracellular acidification: The carboxyl tail length. Biophys J 1993;64:1422–33
46. Morley GE, Taffet SM, Delmar M. Intramolecular interactions mediate pH regulation of connexin43 channels. Biophys J 1996;70:1294–302
47. Duffy HS, Ashton AW, O'Donnell P, et al. Regulation of connexin43 protein complexes by intracellular acidification. Circ Res 2004;94: 215–22
48. Lin JH, Weigel H, Cotrina ML, et al. Gap-junction-mediated propagation and amplification of cell injury. Nat Neurosci 1998;1:494–500
49. Kolb B, Morshead C, Gonzalez C, et al. Growth factor-stimulated generation of new cortical tissue and functional recovery after stroke damage to the motor cortex of rats. J Cereb Blood Flow Metab 2007;27: 983–97
50. Nakase T, Yoshida Y, Nagata K. Enhanced connexin 43 immunoreactivity in penumbral areas in the human brain following ischemia. Glia 2006;54:369–75
51. Scemes E. Modulation of astrocyte P2Y1 receptors by the carboxyl terminal domain of the gap junction protein Cx43. Glia 2008;56:145–53
52. Scemes E, Duval N, Meda P. Reduced expression of P2Y1 receptors in connexin43-null mice alters calcium signaling and migration of neural progenitor cells. J Neurosci 2003;23:11444–52
53. Rohl C, Lucius R, Sievers J. The effect of activated microglia on astrogliosis parameters in astrocyte cultures. Brain Res 2007;1129:43–52
54. Li X, Su V, Kurata WE, et al. A novel connexin43-interacting protein, CIP75, which belongs to the UbL-UBA protein family, regulates the turnover of connexin43. J Biol Chem 2008;283:5748–59
55. Saez JC, Retamal MA, Basilio D, et al. Connexin-based gap junction hemichannels: Gating mechanisms. Biochim Biophys Acta 2005;1711: 215–24
56. Iacobas DA, Urban-Maldonado M, Iacobas S, et al. Array analysis of gene expression in connexin-43 null astrocytes. Physiol Genomics 2003; 15:177–90